

Mechanically driven alloying and grain size changes in nanocrystalline Fe-Cu powders

J. Eckert, J. C. Holzer, C. E. Krill III, and W. L. Johnson

California Institute of Technology, W. M. Keck Laboratory of Engineering Materials 138-78, Pasadena, California 91125

(Received 24 March 1992; accepted for publication 21 September 1992)

Highly supersaturated nanocrystalline $\text{Fe}_x\text{Cu}_{100-x}$ alloys ($10 \leq x \leq 95$) have been prepared by mechanical alloying of elemental crystalline powders. The development of the microstructure is investigated by x-ray diffraction, differential scanning calorimetry, and transmission electron microscopy. The results are compared with data for ball-milled elemental Fe and Cu powders, samples prepared by inert gas condensation, and sputtered films. The deformation during milling reduces the grain size of the alloys to 6–20 nm. The final grain size of the powders depends on the composition of the material. Single-phase fcc alloys with $x \leq 60$ and single-phase bcc alloys with $x \geq 80$ are formed even though the Fe-Cu system exhibits vanishingly small solid solubilities under equilibrium conditions. For $60 \leq x \leq 80$, fcc and bcc solid solutions coexist. The alloy formation is discussed with respect to the thermodynamic conditions of the material. The role of the large volume fraction of grain boundaries between the nanometer-sized crystals, as well as the influence of internal strains and stored enthalpies introduced by ball milling, is critically assessed.

I. INTRODUCTION

The synthesis of metastable phases by mechanical alloying/ball milling has been studied extensively in recent years since it has been shown that this technique is a versatile tool for producing materials far from thermodynamic equilibrium. Much work has been performed on the formation of metastable amorphous, quasicrystalline, and crystalline phases for systems with a negative enthalpy of mixing.^{1–4} For such materials, the phase formation has been explained by both thermodynamic and kinetic arguments.¹ However, mechanical alloying of systems with a positive enthalpy of mixing is far from being well understood. Solid solutions in immiscible systems, such as Fe-Cu,^{5–7} Fe-Ag,⁷ Ag-Cu,⁷ Cu-V,⁸ Cu-W,⁹ and Cu-Ta,¹⁰ have been prepared by mechanical alloying. The formation of these solid solutions is in apparent contrast to what one would expect from the equilibrium phase diagram of these systems.

Recently, it has been shown that nanocrystalline metals and alloys with large excess enthalpies can be obtained by mechanical attrition.^{11–15} It has therefore been suggested that the mechanically stored enthalpy caused by internal strains and the large grain boundary fraction due to the small crystal size in these materials can serve as a driving force for alloy formation.^{7,16} Transmission electron microscopy revealed that by ball milling, the nanocrystalline structure with random orientation of individual grains evolves from dislocation cell structures within shear bands.¹² By further deformation, the dislocation cells/low-angle grain boundaries vanish, leading finally to a fully nanocrystalline powder with a completely random orientation of neighboring grains separated by high-angle grain boundaries.¹² Thus, the details of generation and motion of dislocations under mechanical attrition, as well as their annihilation by recovery and recrystallization, seem to play

a crucial role in the formation and the properties of ball-milled nanocrystalline materials.

In this work, we investigate alloy formation in binary $\text{Fe}_x\text{Cu}_{100-x}$ mixtures ($10 \leq x \leq 95$). Mechanical alloying leads to nanocrystalline solid solutions with drastically extended solubilities. The results are compared with data for ball-milled elemental powders and samples prepared by liquid quenching and evaporation techniques. The alloying process is discussed with respect to the large interfacial area between the small crystals, the mechanically induced strains, and the excess enthalpies produced by milling. The grain size of the alloys depends on the overall composition of the material. For this, a model based on the deformation mechanism during ball milling, including solution hardening during alloying, is inferred, and the influence of grain boundaries and chemical inhomogeneities on the deformation characteristic is critically assessed.

II. EXPERIMENTAL METHODS

Elemental Fe and Cu powders with a purity of 99.9% or better and a particle size of $\leq 100 \mu\text{m}$ were used. The powders were mixed to give the desired average composition and sealed in a vial under an argon atmosphere. The ball milling was performed in a standard Spex 8000 laboratory mill using hardened steel balls and vial with a ball-to-powder weight ratio of 4:1. The vial temperature was kept constant during the experiments by air cooling. After different milling times, the mechanical attrition was interrupted and a small quantity of powder was removed for further characterization. All the handling was done under an argon atmosphere to avoid oxidation.

The x-ray diffraction patterns were taken with a Norelco diffractometer using Ni-filtered $\text{Cu } K\alpha$ radiation ($\lambda = 0.1542 \text{ nm}$). For transmission electron microscopy (TEM) (Philips EM 430 microscope operated at 300 kV),

the powders were mixed with epoxy, and 20–50-nm-thick sections were prepared by diamond-knife microtomy. Chemical analysis of the powders was done by wavelength-dispersive x-ray analysis (WDX) using a JEOL Superprobe 733 operated at 15 kV. The WDX analysis revealed only slight changes in the overall composition of the powders due to wear debris from the milling tools: less than 2 at. % additional Fe was found even after 24 h of milling for all compositions. Thermal analysis was performed in a differential scanning calorimeter (Perkin–Elmer DSC 4) at a heating rate of 20 K/min under flowing argon. After each scan, a subsequent scan was carried out without changing the sample configuration and used as a baseline.

III. RESULTS

A. Progress of phase formation and development of microstructure

The x-ray diffraction patterns for $\text{Fe}_{30}\text{Cu}_{70}$, $\text{Fe}_{70}\text{Cu}_{30}$, and $\text{Fe}_{90}\text{Cu}_{10}$ powders after different milling times are shown in Figs. 1(a)–1(c). For $\text{Fe}_{30}\text{Cu}_{70}$, the initially sharp diffraction lines of elemental Cu and Fe broaden significantly during milling and are reduced in intensity. After 8 h, the Fe peaks have completely disappeared and only fcc peaks remain [Fig. 1(a)]. A similar development is observed for $\text{Fe}_{90}\text{Cu}_{10}$. The fcc Cu peaks disappear completely after 8 h and only bcc peaks are visible after 24 h of milling [Fig. 1(c)]. As the intensity of the elemental x-ray lines is reduced, the diffraction lines of the solid solutions are displaced, compared to the Bragg peaks of pure Cu and Fe, thus indicating true alloying (see below). For $\text{Fe}_{70}\text{Cu}_{30}$, the x-ray lines of Fe and Cu also broaden and decrease in intensity with milling, but both sets of fcc and bcc diffraction lines remain clearly visible, even after extended milling [Fig. 1(b)]. Therefore, a two-phase mixture of fcc and bcc solid alloys forms in this case rather than a homogeneous solid solution.

The microstructure of the mechanically alloyed powders was investigated by TEM. For $x < 60$ and $x > 80$, the selected-area diffraction (SAD) patterns exhibit only the characteristic Debye–Scherrer rings of fcc and bcc structures, respectively. This confirms the interpretation of the x-ray results in terms of single-phase alloys. Figure 2 shows (111) fcc and (110) bcc dark-field images and the corresponding SAD patterns for fcc $\text{Fe}_{50}\text{Cu}_{50}$ and bcc $\text{Fe}_{90}\text{Cu}_{10}$ powders after 24 h of milling, respectively. The TEM images reveal a very fine-grained microstructure of individual crystals which are separated by high-angle grain boundaries (the larger areas visible in Fig. 2 are composed of several individual grains).

The progress of alloying is illustrated in Fig. 3, which shows the change of the fcc and bcc lattice parameters for $\text{Fe}_{30}\text{Cu}_{70}$ and $\text{Fe}_{90}\text{Cu}_{10}$, respectively, as a function of milling time. The lattice parameters were calculated using Cohen's method¹⁷ and the extrapolation function $\cos^2 \Theta / \sin \Theta$. Between 2 and 8 h, both the fcc and bcc lattice parameters increase strongly and approach a saturation value with longer processing. This indicates that alloying takes place mainly within the first 8 h, reaching a steady

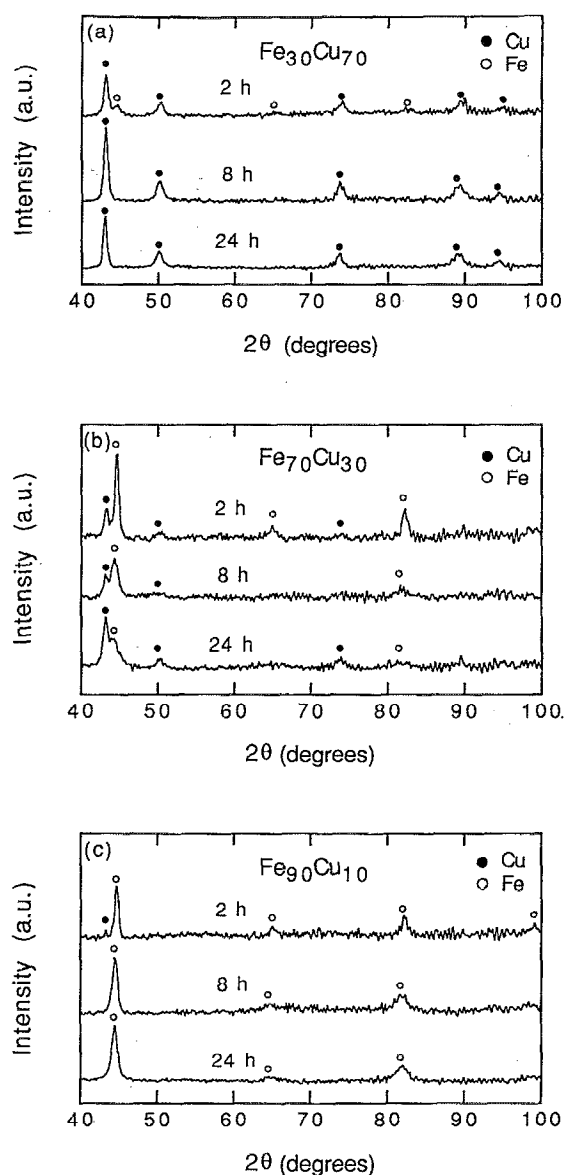


FIG. 1. X-ray diffraction patterns for (a) $\text{Fe}_{30}\text{Cu}_{70}$, (b) $\text{Fe}_{70}\text{Cu}_{30}$, and (c) $\text{Fe}_{90}\text{Cu}_{10}$ after different milling times are shown.

state after 24 h. This is consistent with the results shown in Fig. 1: the x-ray peaks of unreacted elemental Fe and Cu are no longer visible after 8 h of milling.

The x-ray diffraction data as a function of milling time were used to gain further insight into the refinement of the microstructure and the increase of atomic-level strain during mechanical alloying. The initially sharp diffraction lines of fcc Cu and bcc Fe broaden significantly during milling, as mentioned above (Fig. 1). This is due to two effects: finite size broadening and atomic-level strain broadening. To separate these two effects we analyzed the full width at half maximum (FWHM) of the Bragg peaks as a function of the diffraction angle. The size broadening profile was approximated by a Cauchy function and the strain broadening profile by a Gaussian function.¹⁸ The functional relationship between the observed peak FWHM and

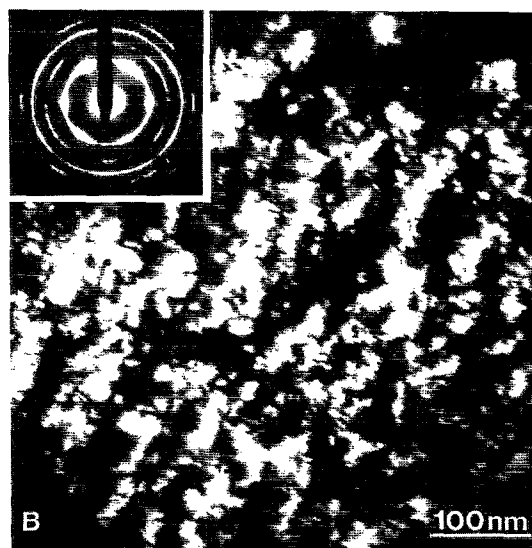
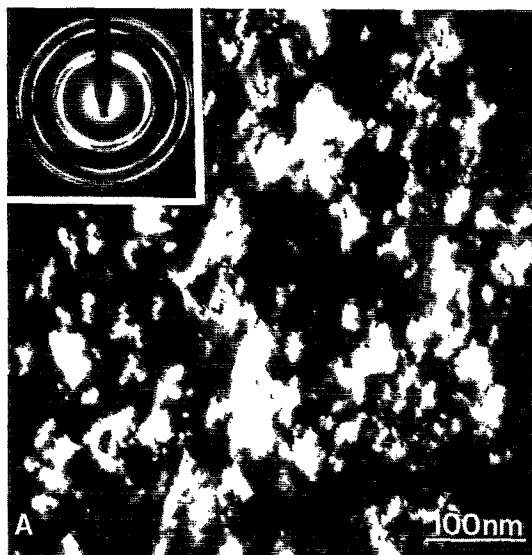


FIG. 2. Dark-field TEM images and corresponding selected area diffraction patterns for (a) $\text{Fe}_{30}\text{Cu}_{30}$ and (b) $\text{Fe}_{90}\text{Cu}_{10}$ after 24 h of milling are shown.

the size and strain FWHMs can then be calculated from the convolution of a Cauchy and a Gaussian function.

Converting the diffraction angle 2θ to the reciprocal space variable $s = 2 \sin \theta / \lambda$, one can show¹⁸ that the peak broadening $(\delta s)_{\text{size}}$ due to size effects is independent of s , while the strain broadening $(\delta s)_{\text{strain}}$ is proportional to s . Thus, the dependence of the measured peak width $(\delta s)_0$ on s , determined after $K\alpha_2$ intensity and instrumental broadening corrections, enables the broadening contributions of size and strain effects to be separated. Furthermore, by substituting the functional dependence of $(\delta s)_{\text{size}}$ and $(\delta s)_{\text{strain}}$ on s into an approximation for a Cauchy/Gaussian convolution, one finds that the relationship be-

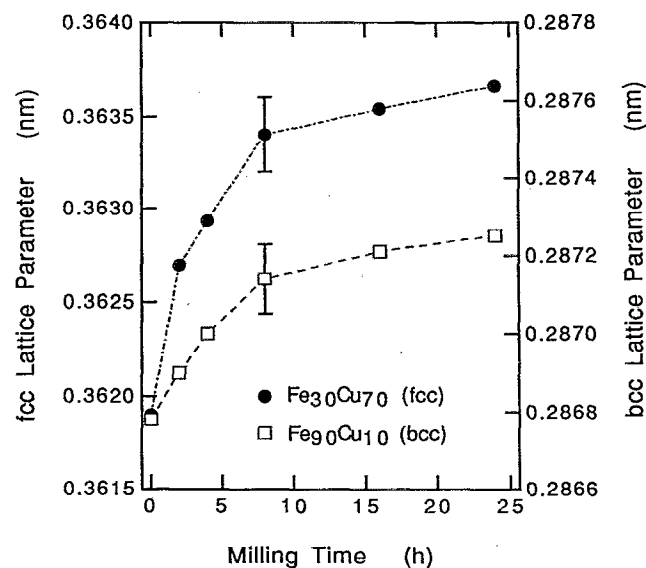


FIG. 3. Lattice parameters for $\text{Fe}_{30}\text{Cu}_{70}$ and $\text{Fe}_{90}\text{Cu}_{10}$ versus milling time are shown.

tween the volume-average grain size d and the rms atomic-level strain $\langle e \rangle^{1/2}$ is¹⁸

$$1/(\delta s)_0 \approx d - 6.25 \langle e^2 \rangle d [s/(\delta s)_0]^2. \quad (1)$$

By performing a least-squares fit to $1/(\delta s)_0$ plotted against $[s/(\delta s)_0]^2$ for all the measured peaks of a sample, we are able to determine d and $\langle e^2 \rangle^{1/2}$.

Figure 4 shows the reduction of grain size and the increase in rms atomic-level strain with increasing milling time for $\text{Fe}_{30}\text{Cu}_{70}$ and $\text{Fe}_{90}\text{Cu}_{10}$ as typical examples. In the early stages of milling, the grain size decreases rapidly to less than 20 nm and approaches a steady-state value of about 12 nm for $\text{Fe}_{30}\text{Cu}_{70}$ and 10 nm for $\text{Fe}_{90}\text{Cu}_{10}$ after 24 h of milling. Simultaneously, the rms atomic-level strain increases to a maximum value of about 0.3% for $\text{Fe}_{30}\text{Cu}_{70}$ and 0.8% for $\text{Fe}_{90}\text{Cu}_{10}$ after 8 h of milling. With extended processing, the strain decreases again and approaches a steady-state value for long milling times/small grain sizes. The observed strain values are comparable to the values found for other ball-milled metals and alloys.⁷⁻¹⁵ In particular, a maximum in the rms strain has also been reported for ball-milled elemental Ru and the CsCl-type compound AlRu.¹¹

Further information on the progress of alloying can be obtained by differential scanning calorimetry (DSC). Figure 5 shows the DSC traces after different milling times for $\text{Fe}_{30}\text{Cu}_{70}$ as a typical example. Milling for 2 h results in a broad exothermic reaction that starts at about 370 K and is almost completed at 870 K. With increasing milling time, two exothermic maxima at ~ 680 K and ~ 750 K become more pronounced. X-ray diffraction of samples heated above the first maximum reveals that phase separation occurs during this exotherm. Simultaneously, the grain sizes of Fe and Cu increase to about 20 nm, and the strain drops to about 0.1%. During heating to 870 K, further grain

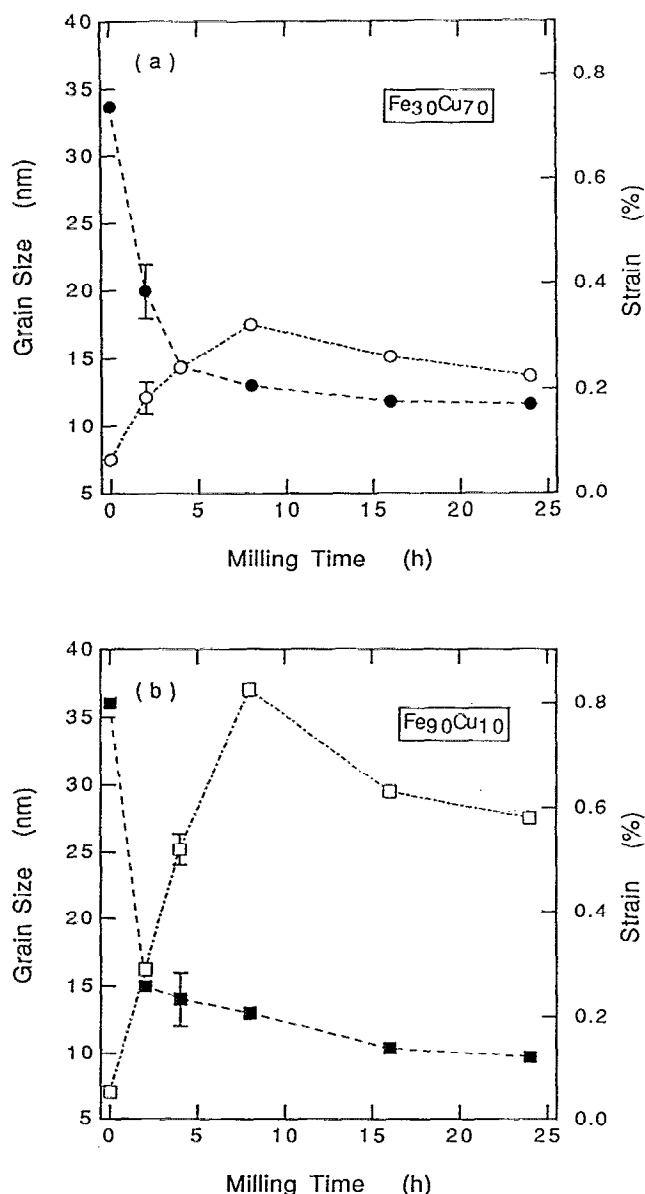


FIG. 4. Average grain size (filled symbols) and atomic-level strain (open symbols) for (a) Fe₃₀Cu₇₀ and (b) Fe₉₀Cu₁₀ versus milling time are shown.

growth and strain release occurs. Similar results have been observed for all compositions (for further details see Ref. 19).

Integrating the DSC traces from 320 to 870 K yields an estimate for the total stored enthalpy introduced during milling. The stored enthalpy as a function of milling time is shown in Fig. 6 for Fe₃₀Cu₇₀ and Fe₉₀Cu₁₀ as typical examples. It increases to a maximum value of about 8.5 kJ/mol for Fe₃₀Cu₇₀ and 5.8 kJ/mol for Fe₉₀Cu₁₀ after 8 h of milling. Further milling/refinement of the microstructure results in a decrease of the heat release for both compositions. Similar results have been reported for other ball-milled nanocrystalline powders.^{11,12}

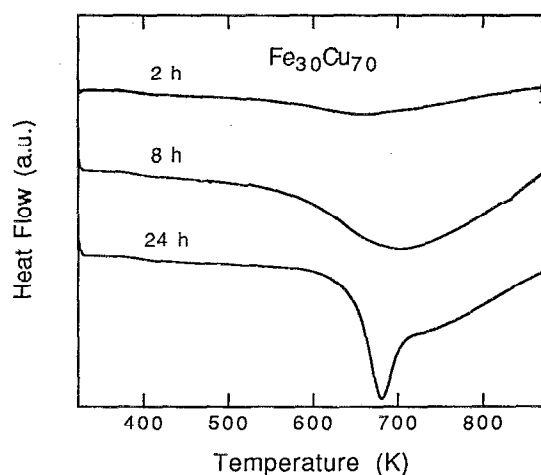


FIG. 5. DSC scans for Fe₃₀Cu₇₀ after different milling times (heating rate 20 K/min) are shown.

B. Formation ranges of fcc and bcc solid solutions and compositional dependence of grain size and lattice

The x-ray diffraction and TEM investigations reveal that mechanical alloying results in a drastically enhanced mutual solubility for the Fe-Cu system (Figs. 1 and 2). This is illustrated in Fig. 7, which shows the compositional dependence of the atomic volume in terms of the Wigner-Seitz cell volume for fcc and bcc solid solutions in 24 h milled samples. For $x < 60$, the atomic volume increases continuously from the value of pure Cu with increasing Fe content. For Fe-rich samples ($x \geq 80$), the atomic volume increases with increasing Cu content. This demonstrates that true alloying takes place for Cu-rich and Fe-rich powders, respectively. In the two-phase region from 60 to 80 at.% Fe, the atomic volume of the fcc phase decreases with the increasing overall Fe content. The data suggest that about 10–30 at.% Fe is dissolved in the fcc phase in this regime. On the other hand, the atomic volume of the bcc phase increases in the two-phase region with the increasing overall Cu content, indicating that even more than 20 at.% Cu is dissolved in the bcc phase.

Our measured Wigner-Seitz cell volumes exhibit a similar compositional dependence as the data reported for other mechanically alloyed powders,^{5–6} but are in general smaller for $x \geq 20$. On the other hand, for fcc solid solutions, our atomic values are larger than the values for samples obtained by liquid quenching²⁰ and evaporated alloys.^{21,22} For bcc solid solutions, the data reported for the other preparation techniques exceed our measured values. Comparison of the data suggests that the atomic volume and the formation ranges of the alloys are very sensitive to experimental conditions, even for samples produced by the same preparation technique. The increase in the bcc atomic volume with increasing Cu content has been claimed to indicate a tendency to instability of the bcc phase upon alloying that could trigger the phase transition from the bcc to the fcc structure.²² However, the drastic volume expansion reported by Chien *et al.* for sputtered bcc alloys

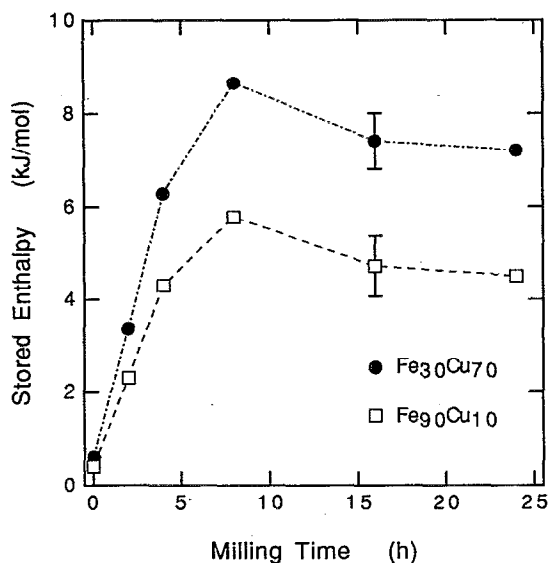


FIG. 6. Stored enthalpy in $\text{Fe}_{30}\text{Cu}_{70}$ and $\text{Fe}_{90}\text{Cu}_{10}$ versus milling time is shown.

in the two-phase region has not been observed in our samples or by any other investigators (Fig. 7).

As mentioned above, an estimate of the positive enthalpy of mixing for Fe-Cu alloys can be obtained by measuring the heat release during heating in the DSC. The maximum total stored enthalpies after 8 h of milling and the residual stored enthalpies after 24 h of milling for var-

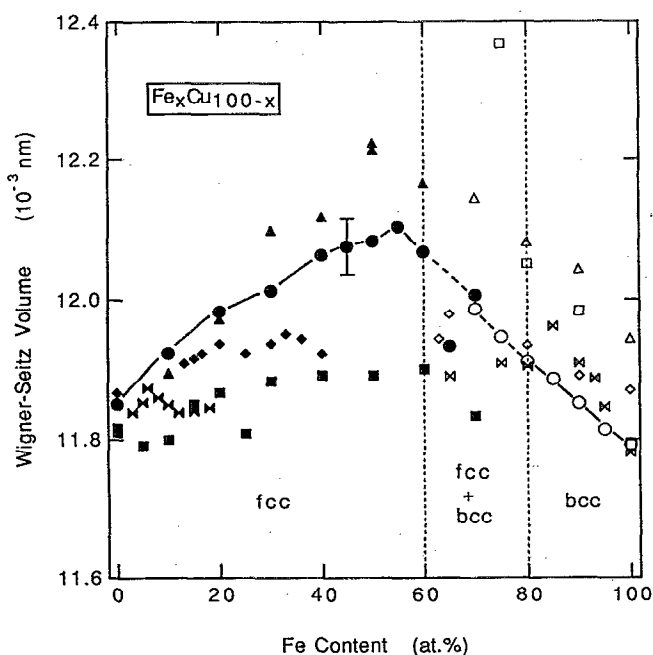


FIG. 7. Shown is the compositional dependence of the Wigner-Seitz cell volume for $\text{Fe}_x\text{Cu}_{100-x}$ alloys: (●, ○) this work after 24 h of milling (▲, △) mechanical alloying (Refs. 5-6), (◀, ▶) liquid quenching (Ref. 20), (◆, ◇) evaporation (Ref. 21), (■, □) evaporation (Ref. 22). Filled symbols refer to fcc alloys and open symbols to bcc alloys.

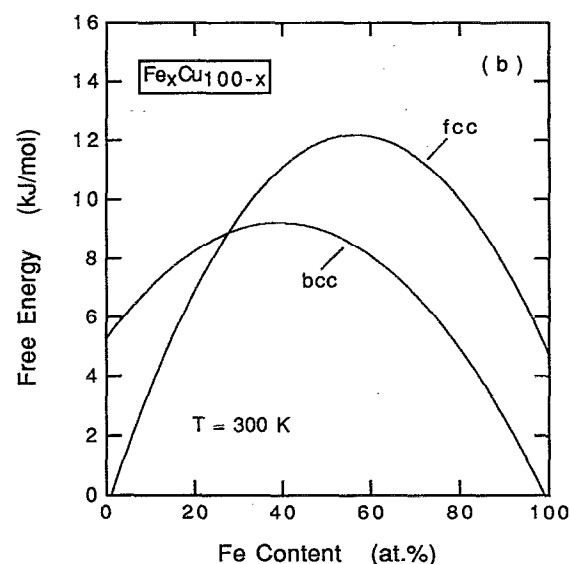
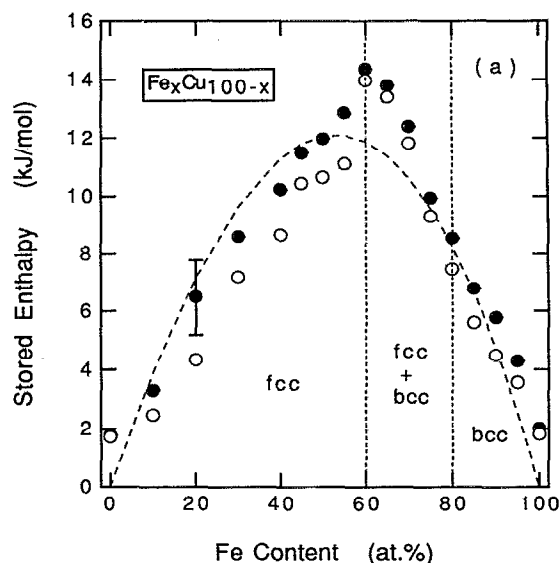


FIG. 8. (a) The maximum total stored enthalpy after 8 h of milling (filled symbols) and the residual total stored enthalpy after 24 h of milling (open symbols) in $\text{Fe}_x\text{Cu}_{100-x}$ powders are shown and compared with the positive enthalpy of mixing (dashed line) calculated using Miedema's model (Ref. 23). (b) Free energies at 300 K for the fcc and the bcc phase calculated from thermodynamic data using the CALPHAD method (Ref. 24) are shown.

ious $\text{Fe}_x\text{Cu}_{100-x}$ powders are shown in Fig. 8(a). The measured enthalpies depend on the overall composition of the samples. Large enthalpies of up to 14 kJ/mol for $\text{Fe}_{60}\text{Cu}_{40}$ are stored in the material. In particular, our maximum value of 11.9 ± 1.3 kJ/mol for $\text{Fe}_{50}\text{Cu}_{50}$ agrees with the value reported by Yavari for the same alloy (10.8 kJ/mol).⁶ The dashed line in Fig. 8(a) refers to the positive enthalpy of mixing ΔH_{mix} calculated using Miedema's model.²³ The measured enthalpies reach or even exceed the ΔH_{mix} values, indicating that mechanical alloying can in fact store enough enthalpy in the material to overcome the positive enthalpy of mixing in this system.

The measured formation ranges of fcc and bcc alloys

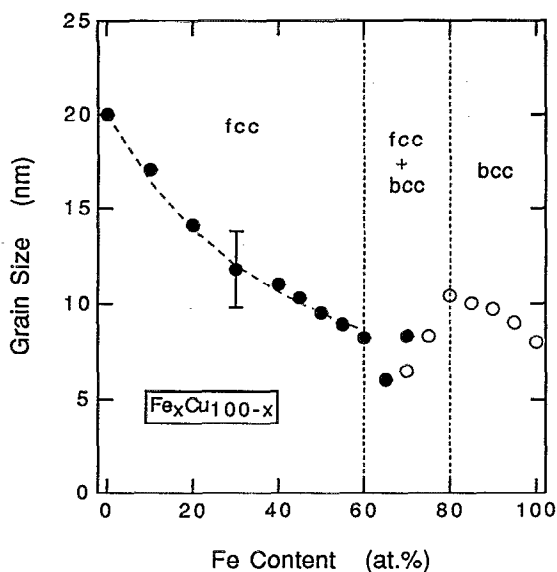


FIG. 9. Shown is the average grain size obtained by ball milling for $\text{Fe}_x\text{Cu}_{100-x}$ powders after 24 h of milling versus the Fe content.

differ from the ranges one would expect from the free energy curves at 300 K for metastable fcc and bcc solid solutions calculated from thermodynamic data using the CALPHAD method²⁴ [Fig. 8(b)]. We found single-phase fcc alloys in the concentration range $30 \leq x \leq 60$, although the bcc phase has a lower calculated free energy than the fcc phase for $x \geq 30$. For Fe-rich compositions ($x \geq 80$), the measured enthalpies agree reasonably well with the calculated curves, but according to the calculated free energy of the bcc phase, one would expect an even larger extension of the bcc phase field. In addition, the observed two-phase region between 60 and 80 at.% Fe disagrees with the calculated free energy curves. This suggests that the mechanically alloyed powders cannot be described by a metastable equilibrium according to the calculated free energy curves. It is not yet clear why a two-phase mixture rather than single-phase alloys form for $60 \leq x \leq 80$, for the measured enthalpy release in this region would be sufficient for complete alloying, according to the thermodynamic calculations. Further experiments are under way to clarify these effects.

Independent of the overall composition, the refinement of the microstructure during milling is qualitatively the same for all samples investigated. The final grain sizes determined from x-ray diffraction and TEM vary between 6 and 20 nm, similar to the grain sizes reported for other ball-milled metals and alloys⁷⁻¹⁵ and to data reported for Fe-Cu alloys prepared by mechanical alloying^{5,6} and inert gas condensation.²⁵ The ultimate grain size depends on the composition of the material. This is illustrated in Fig. 9, showing the final average grain size for $\text{Fe}_x\text{Cu}_{100-x}$ powders after 24 h of milling. Whereas the grain size is reduced to only 20 nm for pure Cu, it decreases to values below 10 nm for Fe-rich fcc solid solutions. On the other hand, a slight increase of the average grain size with increasing Cu content is observed for bcc alloys. In the two-phase region

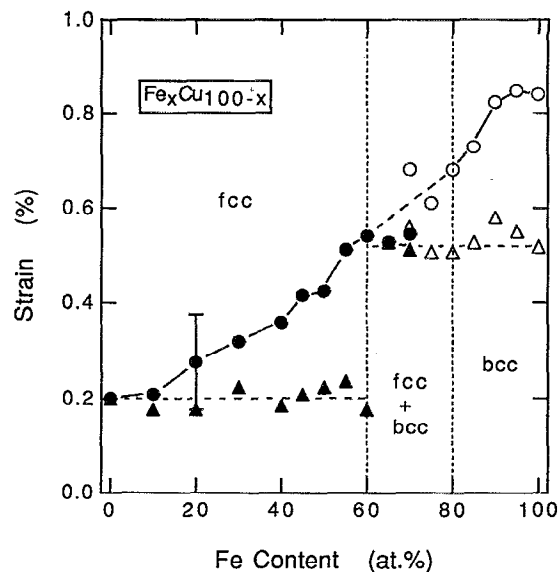


FIG. 10. Atomic-level strain for $\text{Fe}_x\text{Cu}_{100-x}$ powders is shown after 8 h (circles) and 24 h (triangles) of milling versus the Fe content.

between 60 and 80 at.% Fe, the data indicate a decrease in grain size with increasing Fe content in the fcc phase, and with increasing Cu content in the bcc phase. The observed compositional dependence of the grain size demonstrates that the alloy composition strongly affects the final grain size.

The compositional dependence of the maximum atomic-level strain after 8 h of milling and the residual strain after milling for 24 h are shown in Fig. 10. The maximum rms strain increases significantly with increasing Fe content for fcc solid solutions. For bcc alloys, the strain decreases with increasing Cu content. However, the residual strain after 24 h milling seems to be independent of composition: all fcc solid solutions exhibit a strain level of about 0.2%, while for bcc alloys the residual strain is about 0.5%. These values are typical for ball-milled elemental Cu and Fe powders, respectively.¹²⁻¹⁵ It is interesting to note that no significant strain release after extended milling is observed for fcc solid solutions in the two-phase region.

IV. DISCUSSION

A. Mechanism of alloying and formation ranges of fcc and bcc alloys

During milling, the grain size of the elemental Fe and Cu powders decreases to the nanometer scale. Simultaneously, the lattice strain is enhanced. Our results indicate that alloy formation occurs when the Fe and Cu grain sizes are in the range of 10–20 nm and that the resulting fcc and bcc alloys have similar final grain sizes. It has been suggested that the enthalpy stored in the large grain boundary area could serve as a driving force for alloying.^{7,16} However, the alloy phases are also nanocrystalline. Thus, only the chemical component of the interfacial energy can serve as a driving force for alloying. An estimate of the possible reduction of the interfacial energy due to alloying yields a

value of about 1.7 kJ/mol for Fe₅₀Cu₅₀.⁶ The stored enthalpy caused by the heavy deformation of the powders can be as large as 2 kJ/mol.¹ Thus, the contributions of alloying at the interface and mechanical deformation yield a total stored enthalpy of about 3.7 kJ/mol, which is roughly three times too small to overcome the calculated positive enthalpy of mixing of 12 kJ/mol for Fe₅₅Cu₄₅.²³ Such a value could explain alloy formation for samples with only about 10 at.% Fe in Cu or Cu in Fe [Fig. 8(a)]. However, the stress fields of dislocations also raise the free energy of the elemental powder mixture and can, therefore, serve as a driving force for alloying.²⁶ The stress acting on a solute atom located at a distance r from a dislocation core is given by

$$\sigma = -Gb(1+\nu)\sin\Theta/3\pi(1-\nu)r, \quad (2)$$

where G is the shear modulus, b the Burgers vector, ν the Poisson ratio of the host metal, and Θ the angle about the glide plane.²⁶ The effect of stress upon the chemical potential μ of a solute atom is given by

$$\Delta\mu = -\sigma V_m \quad (3)$$

where V_m is the molar volume of the solute atom.²⁷ Thus, tensile stresses, as typical for high dislocation densities,²⁸ reduce the chemical potential and lead to an enhanced solubility. The solubility enhancement x/x_0 is given by

$$x/x_0 = \exp(-\Delta\mu/RT) = \exp(-\sigma V_m/RT), \quad (4)$$

where x_0 is the equilibrium solubility, R is the gas constant, and T is the temperature.²⁹ For a typical dislocation density of 10^{12} cm^{-2} (Ref. 1), it follows that there is approximately one dislocation within a grain of 10 nm diameter. For a temperature of 400 K and a grain size of 10 nm ($r=5 \text{ nm}$), this yields a solubility enhancement of $x/x_0=3.4$ for Fe in Cu and of 5.8 for Cu in Fe, respectively. The solubility enhancement depends strongly on r —i.e., a stacking fault with a typical width of 3 nm (Ref. 28) reduces the average r , resulting in an even larger solubility enhancement of $x/x_0=20$ for Fe in Cu. This suggests that the high dislocation density in ball-milled powders^{11–15} causes a drastic increase in the mutual solubility. Together with the excess enthalpy of grain boundaries, this shows that the driving force for alloying, even for concentrated Fe-Cu mixtures, can in fact be provided by milling.

Further support for the important role of the high dislocation density on the alloying process can be derived from the dependence of the rms atomic-level strain on milling time. As shown in Fig. 4, the rms strain increases to a maximum after 8 h of milling and decreases with longer milling/further refinement of the microstructure. Furthermore, the stored enthalpy also exhibits a maximum after 8 h milling (Fig. 6). Concomitantly, the lattice parameter and the grain size have almost reached their steady-state values (Figs. 3 and 4), indicating that most of the alloying has already occurred at this milling time. In general, lattice strain may arise from the size mismatch of the constituents, from an increasing grain boundary fraction,³⁰ or from mechanical deformation.²⁸ Since the size mismatch of Fe and Cu is only 1.5%, this contribution to the measured

strain values is likely to be small. The fraction of grain boundaries increases continuously with decreasing grain size and cannot, therefore, explain the observed maximum and subsequent decrease of the rms strain. However, mechanical deformation could account for this behavior. In the early stages of milling, the dislocation density increases rapidly due to severe plastic deformation. A saturation and subsequent decrease of the rms strain with increasing milling time/decreasing grain size has also been reported for Ru and AlRu and attributed to a reduction in the dislocation density by the annihilation at grain boundaries for very small grain sizes.¹¹ These considerations suggest that the main contribution to the lattice strain is the dislocation density.

B. Formation ranges of fcc and bcc solid solutions

The change of the lattice parameter and the atomic volume with milling time and composition clearly shows that true alloying occurs during milling (Figs. 3 and 7). The expansion of the bcc lattice parameter with the increasing Cu content can be explained by the increasing fraction of the larger Cu atoms and increasing lattice strain. On the other hand, the expansion of the fcc lattice with the increasing amount of smaller Fe atoms can be attributed to elastic strain and magnetovolume effects.⁶ The formation ranges of the solid solutions agree well with the ranges reported by Uenishi *et al.* for mechanically alloyed powders⁵ and with the ranges found for evaporated samples.²² The observed compositional dependence of the atomic volume in the two-phase region is not yet well understood. Our results show that for $60 \leq x \leq 80$, the atomic volume of the fcc phase decreases with the increasing overall Fe content, indicating that the fcc phase is depleted in Fe compared to the overall composition. On the other hand, the atomic volume of the bcc phase is even larger than for single-phase bcc alloys ($x > 80$), indicating an enhanced Cu solubility in the two-phase region. Apparently, the presence of a second phase strongly affects the solubility in Fe-Cu alloys.

The experimentally observed formation ranges of the single-phase alloys are quite different from what one would expect given the calculated free energy curves for this system [Fig. 8(b)]. This suggests that no metastable equilibrium is achieved during milling, which is supported by the compositional dependence of the atomic volume in the two-phase region. For a metastable equilibrium between homogeneous fcc and bcc solid solutions, one would expect two phases with fixed compositions in the two-phase region, and only the relative amounts of both phases should vary with composition. Presumably, the heavily deformed powders have a higher free energy than under metastable equilibrium conditions, resulting in different formation ranges than expected from the calculated free energy curves [Fig. 8(b)]. Other possible explanations that could account for the difference between the measured and the calculated formation ranges are magnetic effects upon alloying in these highly supersaturated alloys and additional contributions due to the grain boundary energy in nanocrystalline materials. These effects are not included in the

thermodynamic calculations. They could alter the calculated free energy curves for the fcc and bcc phases, resulting in different metastable formation ranges of the super-saturated solid solutions.

C. Compositional dependence of grain size and strain

Ball milling reduces the grain size of the powders to the nanometer scale. The final grain sizes are comparable to the grain sizes reported for mechanically alloyed Fe-Cu^{5,6} and other ball-milled metals and alloys⁷⁻¹⁵ as well as to data reported for samples prepared by inert gas condensation.²⁵ The mechanism for producing nanocrystalline powders by ball milling is governed by the severe plastic deformation introduced during milling.¹¹⁻¹³ The grain size saturates at a steady-state value and no further refinement occurs. For pure metals, we have suggested that the ultimate grain size achievable by milling is determined by the minimum grain size that can sustain a dislocation pileup within a grain and by the rate of recovery during milling.¹⁵ An estimate of the minimum dislocation separation in a pileup L is obtained from the equilibrium between the repulsive force between dislocations and the externally applied force:

$$L = 3Gb/\pi(1-\nu)h, \quad (5)$$

with shear modulus G , Burgers vector b , Poisson ratio ν , and hardness of the material h .³¹ This gives a lower bound for the grain size of pure metals and reveals that a small grain size itself provides a limit for further plastic deformation via dislocation motion and, therefore, for further grain size refinement by milling (for details see Ref. 15).

Figure 9 shows that the final grain size of the fcc Fe-Cu alloys decreases considerably with the increasing Fe content. This can be explained by considering the solution hardening effects upon alloying. In general, the additions of a second element to a pure metal increase the strength and the hardness of the material,²⁸ resulting in a smaller L than for a pure metal and, therefore, in a smaller final grain size obtained by milling. For $x < 60$, the compositional dependence of the grain size d can be fitted best by a relation of the type

$$d = 1/(A + Bx), \quad (6)$$

as shown by the dashed line in Fig. 9. This linear compositional dependence for $1/d$ is characteristic of dislocation locking mechanisms where dislocations are either chemically locked by segregated solute atoms at stacking faults in the fcc lattice³² or by elastic locking due to the atomic size mismatch of the constituents.³³ Since the difference in the atomic sizes of Cu and Fe atoms is only 1.5%, the locking effect due to the size mismatch is very small. Therefore, the major contribution to the solute hardening is likely to be due to segregation of Fe atoms at stacking faults in the fcc lattice. The dislocations become immobile due to the decoration with solute atoms and no further plastic deformation by dislocation motion can occur. Hence, the grain size reaches a steady-state value. It is interesting to note that the observed linear compositional

dependence of $1/d$ is even stronger than the $x^{2/3}$ dependence typical for solid solution hardening caused by the dislocation friction in conventional highly concentrated alloys.³⁴

However, this explanation holds only for single-phase fcc alloys with $x < 60$. The compositional dependence of the grain size for the bcc phase cannot be explained by a solution hardening model. As the Cu content in the bcc phase increases, solid solution hardening would predict a decrease in grain size, as described above for the fcc phase. Possible explanations for the compositional dependence of the grain size for the bcc phase include the stabilization and locking of normally unstable stacking faults in the bcc lattice of nanocrystalline powders¹⁹ (which would reduce the number of mobile dislocations) or a change in the dislocation density by a change of the annihilation behavior at grain boundaries. For samples in the two-phase region, additional contributions due to the inhomogeneity of the material consisting of grains with different lattices and compositions might also affect the dislocation formation and annihilation characteristics. It is well known that grain boundaries can act as sources and sinks for dislocations.³⁵ Therefore, the formation of additional secondary grain boundary dislocations³⁶ at fcc/bcc interfaces could strongly affect the deformation behavior and, therefore, the final grain size of the powders. Furthermore, Fe-Cu is a system with a tendency for interfacial segregation.³⁷ Hence, it is possible that the grain boundary regions are enriched in Cu or Fe in comparison to the bulk of a grain. This might affect the formation and annihilation of dislocations at the grain boundaries, since the image stresses acting on dislocations near the interface between two grains strongly depend on the nature of the grains and the mechanical properties of the phases in contact.³⁵ Hence, compositional variations from the grain interior to the grain boundary due to segregation effects could affect the behavior of the grain boundaries as sources and sinks for dislocations. Further experiments are necessary to gain more insight into these processes for an understanding of the grain size changes for $x > 60$.

Mechanical alloying/ball milling enhances the lattice strain considerably. As shown in Fig. 10, the maximum rms atomic-level strain in the solid solutions after 8 h of milling depends on composition and increases with the increasing Fe content. It has been argued above that the strain is caused mainly by the dislocation density introduced during milling, which, as we suggested, is closely related to the ultimate grain size. The compositional dependence of the strain correlates well with the measured grain sizes (Fig. 9): the higher the rms strain, the smaller the grain size. The decrease of the rms strain after 24 h of milling is likely due to the annihilation of dislocations at grain boundaries for very small grain sizes by dynamic recovery.^{11,12} This agrees with the finding that the stored enthalpy of the powders—which is mainly associated with the dislocation density—decreases for long milling times/very small grain sizes (Figs. 6 and 8). It is interesting to note that the residual strain after extended milling is nearly independent of composition and reaches values that are

typical for ball-milled pure metals (Fig. 10). This proves that the size mismatch of Cu and Fe atoms does not play a significant role for fully alloyed homogeneous powders, since if it were, one would expect a compositional dependence of the residual strain on the Fe and Cu content of the samples.³⁸ The fact that no significant strain release is detected for fcc alloys in the two-phase region suggests that the harder bcc phase in these powders could at least partially prevent dislocation annihilation at grain boundaries, similar to what is known for conventional polycrystalline materials consisting of soft and hard regions.³⁵

V. CONCLUSIONS

We have shown that mechanical alloying of binary Fe-Cu powder mixtures leads to the formation of nanocrystalline single-phase fcc solid solutions with up to 60 at.% Fe in Cu and single-phase bcc solid solutions with up to 20 at.% Cu in Fe. Between 60 and 80 at.% Fe, both phases coexist. The alloy formation can be explained by an enhanced solubility due to the high dislocation density during the initial stages of milling of the nanocrystalline powders. The enthalpy stored in the grain boundaries may also assist the alloying, but this effect alone cannot account for the drastic solubility extension. The ultimate grain size of the powders varies between 6 and 20 nm and scales with the overall composition of the material. This has been explained by the underlying mechanism of plastic deformation via dislocation motion, including solute hardening effects during milling and the influence of grain boundaries on the deformation characteristics.

The results reveal that the details of dislocation formation and motion are essential for understanding the alloying process and the characteristics of mechanically alloyed nanocrystalline powders. Further investigations, such as thermal analysis, TEM, Mössbauer studies and measurements of magnetic properties, are under way to gain a better insight into the details of the phase formation and stability of these materials.³⁹

ACKNOWLEDGMENTS

This work was supported by the U.S. Department of Energy (DOE Contract No. DEFG0386ER45242). Special thanks are given to P. Carpenter and C. Garland for technical assistance, and to Y. R. Abé, R. Birringer, and B. Fultz for stimulating discussions and effective cooperation.

¹W. L. Johnson, *Prog. Mater. Sci.* **30**, 81 (1986).

²L. Schultz, *Mater. Sci. Eng.* **97**, 15 (1988).

³J. Eckert, L. Schultz, and K. Urban, *Appl. Phys. Lett.* **55**, 117 (1988).

⁴E. Ivanov, T. Grigorieva, G. Golubkova, V. Boldyrev, A. B. Fasman, S. D. Mikhailenko, and O. T. Kalinina, *Mater. Lett.* **7**, 51 (1988).

⁵K. Uenishi, K. F. Kobayashi, S. Nasu, H. Hatano, K. N. Ishihara, and P. H. Shingu, *Z. Metallk* **83**, 132 (1992).

⁶A. R. Yavari, P. J. Desré, and T. Benamer, *Phys. Rev. Lett.* **68**, 2235 (1992).

⁷P. H. Shingu, K. N. Ishihara, K. Uenishi, J. Kuyama, and S. Nasu, in *Solid State Powder Processing*, edited by A. H. Clauer and J. J. de Barbadillo (The Minerals, Metals and Materials Society, Cincinnati, OH, 1990), p. 21.

⁸T. Fukunaga, M. Mori, K. Inou, and U. Mizutani, *Mater. Sci. Eng. A* **134**, 863 (1991).

⁹E. Gaffet, C. Louison, M. Harmelin, and F. Faudet, *Mater. Sci. Eng. A* **134**, 1410 (1991).

¹⁰T. Fukunaga, K. Nakamura, K. Suzuki, and U. Mizutani, *J. Non-Cryst. Solids* **117/118**, 700 (1990).

¹¹E. Hellstern, H. J. Fecht, Z. Fu, and W. L. Johnson, *J. Appl. Phys.* **65**, 305 (1989).

¹²H. J. Fecht, E. Hellstern, Z. Fu, and W. L. Johnson, *Adv. Powder Metall.* **1**, 11 (1989).

¹³J. S. C. Jang and C. C. Koch, *Scr. Metall. Mater.* **24**, 1599 (1990).

¹⁴J. Eckert, J. C. Holzer, C. E. Krill III, and W. L. Johnson, *Mater. Sci. Forum* **88-90**, 505 (1992).

¹⁵J. Eckert, J. C. Holzer, C. E. Krill III, and W. L. Johnson, *J. Mater. Res.* **7**, 1751 (1992).

¹⁶T. Shen, K. Y. Wang, M. X. Quan, and J. T. Wang, *Mater. Sci. Forum* **88-90**, 391 (1992).

¹⁷B. D. Cullity, *Elements of X-ray Diffraction*, 2nd ed. (Addison-Wesley, Reading, MA, 1978), p. 363.

¹⁸H. P. Klug and L. Alexander, *X-ray Diffraction Procedures for Polycrystalline and Amorphous Materials*, 2nd ed. (Wiley, New York, 1974), p. 661.

¹⁹J. Eckert, R. Birringer, J. C. Holzer, C. E. Krill III, and W. L. Johnson, in *Structure and Properties of Interfaces in Materials*, edited by W. T. Clark, U. Dahmen, and C. L. Briant (Mater. Res. Soc., Pittsburgh, PA, 1992), Vol. 238, p. 739.

²⁰W. Klement, Jr., *Trans. AIME* **233**, 1180 (1965).

²¹K. Sumiyama, T. Yoshitake, and Y. Nakamura, *J. Phys. Soc. Jpn.* **53**, 3160 (1984).

²²C. L. Chien, S. H. Liou, D. Kofalt, W. Yu, T. Egami, and T. R. McGuire, *Phys. Rev. B* **33**, 3247 (1986).

²³A. K. Niessen, F. R. de Boer, R. Boom, P. F. de Châtel, W. C. M. Mattens, and A. R. Miedema, *CALPHAD* **7**, 51 (1983).

²⁴L. Kaufman, *CALPHAD* **2**, 117 (1978).

²⁵U. Herr, J. Jing, U. Gonser, and H. Gleiter, *Solid State Commun.* **76**, 197 (1990).

²⁶J. C. M. Li, R. Oriani, and L. S. Darken, *Z. Phys. Chem. Neue Folge* **49**, 271 (1966).

²⁷D. Hull and D. J. Bacon, *Introduction to Dislocations* (Pergamon, Oxford, 1984), p. 88.

²⁸P. Haasen, *Physical Metallurgy*, 2nd ed. (Cambridge University Press, Cambridge, 1986), p. 266.

²⁹D. A. Porter and K. E. Easterling, *Phase Transformations in Metals and Alloys* (Van Nostrand Reinhold, London, 1981), p. 44.

³⁰R. C. Cammarata and R. K. Eby, *J. Mater. Res.* **6**, 888 (1991).

³¹T. G. Nieh and J. Wadsworth, *Scr. Metall. Mater.* **25**, 955 (1991).

³²H. Suzuki and C. S. Barrett, *Acta Metall.* **6**, 156 (1958).

³³A. H. Cottrell, C. S. Hunter, and F. R. N. Nabarro, *Philos. Mag.* **44**, 1064 (1953).

³⁴R. Labusch, *Phys. Status Solidi* **41**, 659 (1970); *Acta Metall.* **20**, 917 (1972).

³⁵J. P. Hirth, *Metall. Trans.* **3**, 3047 (1972).

³⁶R. E. Hook and J. P. Hirth, *Acta Metall.* **15**, 1099 (1967).

³⁷E. D. Hondros and M. P. Seah, in *Physical Metallurgy*, edited by R. W. Cahn and P. Haasen, 3rd ed. (Elsevier Science B. V., Amsterdam, 1983), p. 856.

³⁸T. Egami and Y. Waseda, *J. Non-Cryst. Solids* **64**, 113 (1984).

³⁹H. Ouyang, J. Eckert, and B. Fultz (to be published).